Insulator-Metal Transition and Topological Superconductivity in UTe$_2$ from a First-Principles Calculation

Jun Ishizuka, Shuntaro Sumita, Akito Daido, and Youichi Yanase

Department of Physics, Graduate School of Science, Kyoto University, Kyoto 606-8502, Japan

We theoretically study superconductivity in UTe$_2$, which is a recently discovered strong candidate for an odd-parity spin-triplet superconductor. Theoretical studies for this compound faced difficulty because first-principles calculations predict an insulating electronic state, incompatible with superconducting instability. To overcome this problem, we take into account electron correlation effects by a GGA $+ U$ method and show the insulator-metal transition by Coulomb interaction. Using Fermi surfaces obtained as a function of U, we clarify topological properties of possible superconducting states. Fermi surface formulas for the three-dimensional winding number and three two-dimensional $\mathbb{Z}_2$ numbers indicate topological superconductivity at an intermediate U for all the odd-parity pairing symmetry in the *Immm* space group. Symmetry and topology of superconducting gap nodes are analyzed and the gap structure of UTe$_2$ is predicted. Topologically protected low-energy excitations are highlighted, and experiments by bulk and surface probes are proposed to link Fermi surfaces and pairing symmetry. Based on the results, we also discuss multiple superconducting phases under magnetic fields, which were implied by recent experiments.

A recent discovery of superconductivity in UTe$_2$ [1] is attracting much attention. Distinct differences of UTe$_2$ from other uranium-based ferromagnetic superconductors [2,3] are a rather high superconducting transition temperature $T_c \sim 1.6$ K and a nonmagnetic behavior down to 25 mK [4]. Uniform magnetic susceptibility, magnetization, NMR Knight shift, and $1/T_1 T$ support the proximity of metallic ferromagnetic quantum criticality [1,5,6]. An extremely large upper critical field and re-entrant superconductivity have been observed by high-field experiments [1,7,8]. These observations strongly suggest odd-parity superconductivity induced by ferromagnetic fluctuations. A large specific heat coefficient $\gamma = 117$ mJ K^{-2} mol^{-1} indicates itinerant heavy f electrons [5,9,10]. A large residual value of γ in the superconducting state [1,5] suggests a time-reversal symmetry breaking nonunitary pairing, which is known to exist in ferromagnetic superconducting states. However, a direct transition from a normal to a nonunitary superconducting state is prohibited in the presence of spin-orbit coupling by symmetry because the orthorhombic D_{2h} point group of UTe$_2$ includes only one-dimensional (1D) representations. Experimental studies examining this issue are in progress.

Identifying the topological nature of quantum states has been one of the central issues in modern condensed matter physics. Because odd-parity superconductors are a strong candidate of topological superconductors accompanied by Majorana quasiparticles [11–13], many studies have been focused on the odd-parity superconductivity [14–16]. However, odd-parity superconducting materials are rare. Therefore, identifying topological properties of a fresh and

good platform UTe$_2$ is awaited. A nonmagnetic behavior of UTe$_2$ enables time-reversal invariant (class DIII) topological superconductivity, and a relatively high transition temperature at ambient pressure allows many experimental tools, which were hard to use for ferromagnetic superconductors [2,3]. Theoretically, it is important to specify Fermi surfaces (FSs) to identify topological superconductivity. Topological invariants depend on FSs and some of them can be obtained by FS formulas [11–13].

Information on FSs can also be linked to gap structures of unconventional superconductors, and therefore, it enables us to study pairing symmetry by measurements of low energy excitations [17]. Recent progress in topological theory attached a renewed attention to the gap node. According to modern classification of gapless superconductors [18–21] all the superconducting gap nodes are topologically protected. Thus, the criterion of topological superconductivity and gap nodes based on FSs provides a prediction of bulk and surface measurements, revealing the pairing symmetry and Majorana surface states.

Theoretically, a band structure has been studied for UTe$_2$ from first principles [5]. However, the previously obtained result shows an insulating state with a small gap of 13 meV, which contradicts metallic behaviors in electric resistivity [1,5]. On the other hand, small FSs appear in another first-principles band calculation using the relativistic linearized augmented plane wave method [22]. This is also incompatible with transport measurements [23] indicating a large carrier density, as well as their angle-resolved photoemission spectroscopy (ARPES) detecting large intensities around the R point at the Fermi level [22]. These discrepancies between
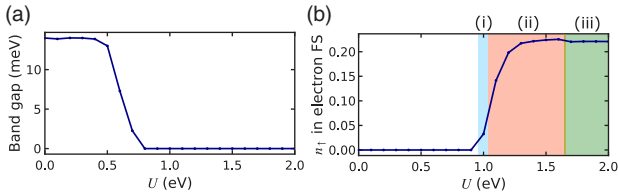
FIG. 1. Coulomb interaction dependence of (a) the band gap at the Fermi level and (b) the electron number n per spin in electron FS. Insulator-metal transition occurs at $U = 1.0$ eV. Metallic states with different topology of FSs are labeled by (i)–(iii).

FIG. 2. (a) First BZ and symmetry points. (b)–(d) FSs of UTe$_2$ by GGA + U for (b) $U = 1.0$ eV [region (i)], (c) $U = 1.1$ eV [region (ii)], and (d) $U = 2.0$ eV [region (iii)]. The electron sheet (cyan and red colors) and the hole sheet (blue and yellow colors) [26].

naive band structure calculations and experiments imply that the Coulomb interaction is crucially important for UTe$_2$.

In this Letter, we provide the first report of a microscopic analysis linking the electronic state and superconductivity in UTe$_2$. We show that the insulator-metal transition is induced by Coulomb interaction. For empirically reasonable values of U, a metallic state is realized, and FSs promise the topological superconductivity for all possible odd-parity pairings. The superconducting gap node ensured by crystal symmetry is predicted by the group theoretical classification combined with topological arguments. In addition, we discuss multiple superconducting phases under magnetic fields along the b axis. A phase transition inside the superconducting phase is proposed.

GGA+U calculation.—The topology of the FS is crucially important for unconventional superconductors, in particular, for the gap structure and topological superconductivity. As we introduced previously, two band structures have been reported. One is insulating [5] and the other is metallic with small FSs [22]. They are clearly contradicting each other and incompatible with experiments. We therefore carry out the density functional theory (DFT) electronic structure calculations in the paramagnetic state using the WIEN2k package [24]. We use the relativistic full-potential linearized augmented plane wave+local orbitals method within the generalized gradient approximation (GGA). In addition to the DFT calculation providing a noninteracting band structure, we introduce the correlation effect of f electrons by the GGA + U method [25]. Details of our band calculations are given in the Supplemental Material [26].

The numerical results are given in Figs. 1–2. The DFT band structure is insulating, and the band gap is 14 meV. Thus, the results are consistent with Ref. [5]. On the other hand, the GGA + U calculation shows the closing of the band gap (Fig. 1), and we observe metallic FSs for $U > 1.0$ eV. It turns out that the correlation effect of f electrons causes an insulator-metal transition. A moderate value of U in the GGA + U calculation may be reliable at low temperatures, where the itinerant f electrons form a heavy fermion state consistent with specific heat measurements [1,5]. A larger U may be appropriate above the
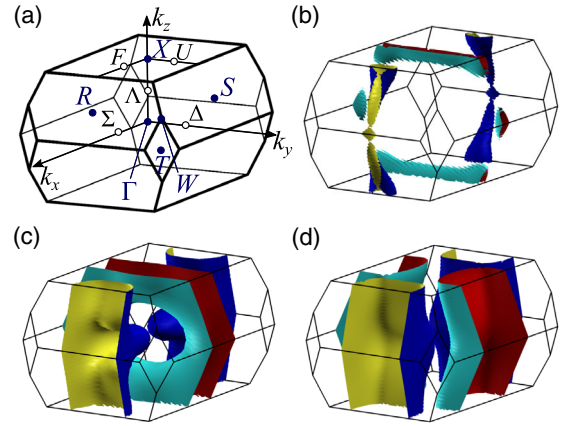
Kondo temperature, where the f electrons are localized. Although we cannot determine the value of U in the framework of the GGA + U method, we can deduce which FS is more appropriate using the comparison with future experiments such as ARPES or quantum oscillations. Furthermore, the GGA + U calculation should be compared with other methods such as GGA + DMFT, which is left as a future work.

The obtained FSs are illustrated in Figs. 2(b)–2(d), each of which shows different topologies labeled by (i)–(iii) in Fig. 1(b). For $U = 1.0$ eV, a tiny electron sheet appears at the Brillouin zone (BZ) boundary around the X point and a tiny hole sheet around the R point. The FSs dramatically increase their volume by an increase of U, involving a topological Lifshitz transition from (i) to (ii). For $U = 1.1$ eV, there appears a ringlike sheet with a heavy effective mass dominated by $j_z = \pm 5/2$ and $\pm 1/2$ components [26]. We also see a cylindrical sheet dominated by $j_z = \pm 5/2$ and $\pm 3/2$ components. The ringlike sheet changes to a two-dimensional (2D) cylindrical sheet at $U = 2.0$ eV, which is shown in Fig. 2(d), with a topological transition at $U \simeq 1.6$ eV. These Fermi sheets consist of $j_z = \pm 5/2$ and $\pm 3/2$ components mixed with $d_{3z^2-r^2}$ and p_y orbitals having a light effective mass [26]. The electron sheet has a large carrier density $n \sim 0.2$ per spin which is compensated by the hole sheet. Thus, we see large FSs occupying 40% of the BZ, in accordance with transport measurements [23]. On the other hand, low carrier density shown in Fig. 2(b) or that obtained by a slight carrier doping to the DFT band structures is incompatible with experiments for UTe$_2$. We also confirmed the insulator-metal transition by the density of states [26]. Then, we notice that the incipient hybridization gap is shifted upwards in energy by 10 meV ($U = 1.0$ eV). The f-electron states with $j = 5/2$ multiplet are dominant around the Fermi level.

TABLE I. Correspondence between high-symmetry points in the original BZ and folded BZ.

Original	Folded
Γ, X	Γ_p: $(0,0,0)$
R	U_p: $[(\pi/a), 0, (\pi/c)]$
S	T_p: $[0, (\pi/b), (\pi/c)]$
T	S_p: $[(\pi/a), (\pi/b), 0]$
W	R_p: $[(\pi/a), (\pi/b), (\pi/c)]$

TABLE II. Occupation number $n(K_i)$ at high symmetry points in the folded BZ and topological invariants (modulo two) corresponding to each topology of FSs. The values $n(K_i) - 180$ are shown below, with $X_p = (\pi/a, 0, 0)$, $Y_p = (0, \pi/b, 0)$, and $Z_p = (0, 0, \pi/c)$.

FSs	Γ_p	X_p	S_p	Y_p	Z_p	U_p	R_p	T_p	$(\omega, \nu_1, \nu_2, \nu_3)$
(i)	6	4	4	8	4	0	4	4	(1,1,1,1)
(ii)	6	0	4	8	4	0	4	8	(1,1,1,1)
(iii)	4	0	4	8	4	0	4	8	(0,0,0,0)

Topological superconductivity.—Here, we discuss topological properties of UTe$_2$, assuming odd-parity superconductivity. We also assume that time-reversal symmetry is preserved in the superconducting phase since this is natural from the group-theoretical perspective as discussed previously. Thus, we focus on the zero-magnetic-field phase, and the putative nonunitary pairing state [1] is beyond our scope.

Topology of odd-parity superconductors is closely related to the topology of FSs. Actually, the parity of various topological invariants is determined by the occupation number at high-symmetry points in the BZ [11–13]. For example, we can identify the parity of the three-dimensional (3D) winding number ω by the following formula:

$$\omega = \frac{1}{2} \sum_{K_i} n(K_i) \quad (\text{mod } 2). \quad (1)$$

Here, K_i runs over eight time-reversal invariant momenta (TRIM) in the 3D BZ, and the occupation number $n(K_i)$ is an even integer due to Kramers degeneracy. Similar formulas are also known for 1D and 2D $\mathbb{Z}_2$ invariants [11–13].

In this Letter, we concentrate on topological invariants related to the (100), (010), and (001) surface states. It should be noted that the size of the primitive cell is doubled because the translation symmetry on these surfaces is compatible with the doubled unit cell. For this reason, we apply the formulas to the folded BZ, instead of the original one. To be specific, the former and the latter BZ correspond to the unit cell formed by $\{a\hat{x}, b\hat{y}, c\hat{z}\}$ and $\{(-a\hat{x} + b\hat{y} + c\hat{z})/2, (a\hat{x} - b\hat{y} + c\hat{z})/2, (a\hat{x} + b\hat{y} - c\hat{z})/2\}$, respectively. The correspondence between high-symmetry points in the two BZs is shown in Table I.

We obtained from the GGA + U results the occupation number at TRIM and corresponding topological invariants (Table II). Here, ν_1, ν_2, and ν_3 are the $\mathbb{Z}_2$ invariants defined on the $k_x = 0$, $k_y = 0$, and $k_z = 0$ planes, respectively. $\mathbb{Z}_2$ invariants defined on the other time-reversal invariant planes are obtained from $(\omega, \nu_1, \nu_2, \nu_3)$, as is the case for topological insulators, and they are trivial in our results.

According to Table II, superconductivity in UTe$_2$ is topologically nontrivial for moderate values of U in the regions (i) and (ii) when the bulk state is gapped. Majorana

states appear on the (100), (010), and (001) surfaces. This is one of the central results of this Letter.

Here we comment on the effect of excitation nodes on the topological superconductivity. Although the winding number ω is ill defined in the gapless states, some of the 2D $\mathbb{Z}_2$ invariants ν_i may still be well defined and the corresponding surface Majorana states may appear. Well-defined topological invariants and surfaces hosting Majorana states are summarized in Table III for each pairing symmetry and FSs. For example, the B_{1u} superconducting state has point nodes on the k_z axis, meaning ν_1 and ν_2 are ill defined. However, ν_3 is well defined and the (100) and (010) surface states are robust. Thus, topological superconductivity can be detected with scanning tunneling microscopy or ARPES for clean surfaces even in gapless superconducting states.

It should be noticed that our results do not exclude the possibility of topological superconductivity for FSs (iii): Indeed, 3D winding number $\omega \in \mathbb{Z}$ can be a finite even integer. By symmetry, this is allowed only for the A_u pairing state [37]. We do not discuss this case because ω depends on detailed properties of superconducting gap function. We also leave the possibility of topological crystalline superconductivity as a future issue.

Topological gap node.—Now we discuss gap structures in the superconducting state of UTe$_2$, using group theory and topology. First, we consider an ordinary classification theory of the superconducting order parameter by the crystal point group [17,38–40]. At zero magnetic field, UTe$_2$ possesses D_{2h} point group symmetry, in which an odd-parity order parameter is classified as one of four irreducible representations (IRs): A_u, B_{1u}, B_{2u}, and B_{3u}. Typical basis functions are shown in Table IV(a). We also consider magnetic fields along the b axis in which UTe$_2$ shows extremely high critical fields and metamagnetic transition [1,7–10]. Then, the symmetry is reduced to C_{2h}^y, which has two odd-parity IRs (A_u and B_u). In this case, the A_u and B_{2u} (B_{1u} and B_{3u}) states are not distinguished by symmetry since they are reduced to the A_u (B_u) state. The correspondence is summarized in Table IV(b).

Although we can speculate gap structures from the order parameter, it is desirable to use the classification of gap structures in terms of symmetry and topology [18–21, 41–47] because symmetry-protected gap nodes are

TABLE III. Gap structures, nontrivial topological indices, and surfaces hosting stable Majorana states for odd-parity pairing states.

	FSs(i,ii)				FSs(iii)		
IR	Gap structure	Topological index	Surfaces	IR	Gap structure	Topological index	Surfaces
A_u	Full gap	$(\omega, \nu_1, \nu_2, \nu_3)$	(100), (010), (001)	A_u	Full gap	$\omega \in 2\mathbb{Z}$	Unpredicted
B_{1u}	Point node (Λ)	ν_3	(100), (010)	B_{1u}	Full gap	Trivial	None
B_{2u}	Point node (Δ)	ν_2	(100), (001)	B_{2u}	Point node (Δ, U)	Trivial	None
B_{3u}	Point node (Σ, F)	ν_1	(010), (001)	B_{3u}	Point node (Σ, F)	Trivial	None

precisely obtained. Detailed results of the topological classification are shown in the Supplemental Material [26]. Using the results, gap structures of UTe$_2$ are obtained for each pairing symmetry and FSs, as shown in Table III.

Considering the FS topology in Figs. 2(b)–2(d), we find that UTe$_2$ is a fully gapped superconductor at zero magnetic field when the order parameter belongs to A_u IR with $U > 1.0$ eV [regions (i)–(iii)], or B_{1u} IR with $U > 1.6$ eV [region (iii)]. Otherwise the superconducting state has some point nodes, whose positions depend on pairing symmetry and they can be distinguished by experiments. In Table V, we show expected anisotropy of thermal conductivity [48], which may determine the symmetry of superconductivity in UTe$_2$.

When the magnetic field is applied along the b axis, superconducting states are classified into A_u or B_u IR. The A_u state of C_{2h}^y can be regarded as a $A_u + B_{2u}$ state, a mixed representation in D_{2h}, while $B_u \uparrow D_{2h} = B_{1u} + B_{3u}$. According to the gap classification in Table S2(b) of the Supplemental Material [26], the A_u state has symmetry-protected point nodes on the k_y axes while the B_u state has a line node on the $k_y = 0$ plane. These results are consistent with speculation from classification of order parameters. Since the spin-triplet order parameter with d vector parallel to the magnetic field does not cause the gap of Bogoliubov quasiparticles, we have only to consider the others. For A_u IR, the allowed bases are $k_x\hat{x}$, $k_z\hat{x}$, $k_x\hat{z}$, and $k_z\hat{z}$, which create point nodes. On the other hand, the B_u

TABLE IV. Classification of odd-parity superconducting order parameters for point groups (a) D_{2h} and (b) C_{2h}^y.

(a) D_{2h} (zero magnetic field)								
IR	E	C_{2z}	C_{2y}	C_{2x}	I	σ_z	σ_y	σ_x	Basis functions
A_u	1	1	1	1	-1	-1	-1	-1	$k_x\hat{x}, k_y\hat{y}, k_z\hat{z}$
B_{1u}	1	1	-1	-1	-1	-1	1	1	$k_y\hat{x}, k_x\hat{y}$
B_{2u}	1	-1	1	-1	-1	1	-1	1	$k_x\hat{z}, k_z\hat{x}$
B_{3u}	1	-1	-1	1	-1	1	1	-1	$k_z\hat{y}, k_y\hat{z}$

(b) C_{2h}^y (magnetic field $\parallel b$)					
IR	(IR)$\uparrow D_{2h}$	E	C_{2y}	I	σ_y	Basis functions
A_u	$A_u + B_{2u}$	1	1	-1	-1	$k_x\hat{x}, k_z\hat{x}, k_y\hat{y}, k_x\hat{z}, k_z\hat{z}$
B_u	$B_{1u} + B_{3u}$	1	-1	-1	1	$k_y\hat{x}, k_x\hat{y}, k_z\hat{y}, k_y\hat{z}$

order parameter of $k_y\hat{x}$ and $k_y\hat{z}$ results in line nodes on the $k_y = 0$ plane.

Multiple phases under magnetic fields.—Experimental data for UTe$_2$ under magnetic fields along the b axis reveal highly unusual behaviors [1,7,8]. The transition temperature shows a nonmonotonic behavior as a function of the magnetic field. It indicates the presence of two superconducting phases: The low-field and high-field phases may be distinguished by symmetry. Considering the gap structure discussed above, we propose the phase diagram in Fig. 3. Because point-nodal superconducting states gain more condensation energy than the line-nodal one, the A_u state may be stable at high magnetic fields, while the $B_u = B_{1u} + B_{3u}$ state may be favored by the spin-orbit coupling at low fields. In this case, the B_{1u} or B_{3u} state is realized at zero magnetic field. The order parameter of both states contains the d vector parallel to the b axis, and therefore, the Knight shift decreases below T_c. This is consistent with a recent NMR experiment [49].

Anisotropy of pairing interaction [50] is also important. Strongly anisotropic ferromagnetic fluctuation may favor the d vector perpendicular to the easy axis. Then, the easy axis along a [1] implies the B_{3u} state at $H = 0$ while the fluctuation along the b axis near the metamagnetic transition [9,10] favors the B_{2u} state. This is consistent with our proposal. Microscopic calculations are desirable for more precise discussions and left for a future study.

Magnetism.—Figures 2(c) and 2(d) show the nesting property of the FSs, and therefore, we expect a magnetic fluctuation with a finite-q nesting vector coexisting with a widely believed ferromagnetic fluctuation. Thus, it is indicated that UTe$_2$ is in the vicinity of the multiple magnetic orderings, and the long-range magnetic order is suppressed by magnetic frustration. This may explain why UTe$_2$ does not undergo magnetic order in contrast to

TABLE V. Expected anisotropy in thermal conductivity at low temperatures for each FSs and pairing symmetry. Anisotropy of fully gapped states cannot be predicted.

FSs	A_u	B_{1u}	B_{2u}	B_{3u}
(i)	Unpredicted	$\kappa_c > \kappa_{a,b}$	$\kappa_b > \kappa_{a,c}$	$\kappa_a > \kappa_{b,c}$
(ii)	Unpredicted	$\kappa_c > \kappa_{a,b}$	$\kappa_b > \kappa_{a,c}$	$\kappa_a > \kappa_{b,c}$
(iii)	Unpredicted	Unpredicted	$\kappa_b > \kappa_{a,c}$	$\kappa_a > \kappa_{b,c}$
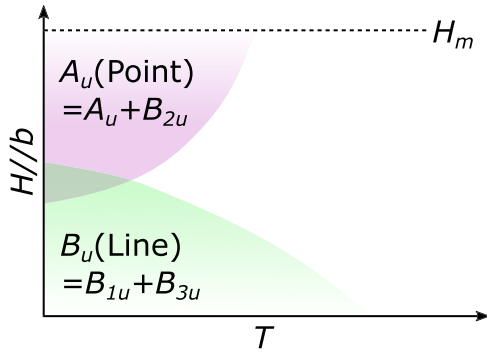
FIG. 3. Schematic phase diagram in the magnetic field (H) and temperature (T) plane. H_m indicates the metamagnetic transition [9,10].

UCoGe and URhGe. A recent first-principles study proposes a similar scenario [51].

Summary and conclusion.—In this Letter, we theoretically investigated the electronic state and superconductivity of UTe$_2$. Using the GGA $+ U$ calculation we clarified the insulator-metal transition due to Coulomb interaction. The metallic band structure for $U > 1.0$ eV is compatible with the metallic conductance and superconducting instability, indicating a crucial role of electron correlation. For moderate U, all the odd-parity superconducting states expected in UTe$_2$ were identified as time-reversal-invariant topological superconductivity. Superconducting gap structures under magnetic fields along the b axis as well as at zero magnetic field were predicted. By this work, bulk and surface excitations characterizing the odd-parity superconductivity in UTe$_2$ are elucidated. Our results pave the way to experimentally determine symmetry of superconductivity and identify intrinsic topological superconductivity which has been rare in nature.

Recently, we become aware of Ref. [52], which reported DFT $+ U$ calculations in both paramagnetic and ferromagnetic states. At their parameters $U = J = 0.51$ eV, an insulating band structure was obtained consistent with our calculations, and insulator-metal transition was not shown. We are also aware of an experimental paper [53] in which point nodes along the a axis are concluded. This implies the B_{3u} state at zero magnetic field consistent with our proposal in Fig. 3.

[1] S. Ran, C. Eckberg, Q.-P. Ding, Y. Furukawa, T. Metz, S. R. Saha, I.-L. Liu, M. Zic, H. Kim, J. Paglione, and N. P. Butch, Science 365, 684 (2019).

[2] D. Aoki and J. Flouquet, J. Phys. Soc. Jpn. 83, 061011 (2014).

[3] D. Aoki, K. Ishida, and J. Flouquet, J. Phys. Soc. Jpn. 88, 022001 (2019).

[4] S. Sundar, S. Gheidi, K. Akintola, A. M. Cote, S. R. Dunsiger, S. Ran, N. P. Butch, S. R. Saha, J. Paglione, and J. E. Sonier, Phys. Rev. B 100, 140502(R) (2019).

[5] D. Aoki, A. Nakamura, F. Honda, D. Li, Y. Homma, Y. Shimizu, Y. J. Sato, G. Knebel, J.-P. Brison, A. Pourret, D. Braithwaite, G. Lapertot, Q. Niu, M. Vališka, H. Harima, and J. Flouquet, J. Phys. Soc. Jpn. 88, 043702 (2019).

[6] Y. Tokunaga, H. Sakai, S. Kambe, T. Hattori, N. Higa, G. Nakamine, S. Kitagawa, K. Ishida, A. Nakamura, Y. Shimizu, Y. Homma, D. Li, F. Honda, and D. Aoki, J. Phys. Soc. Jpn. 88, 073701 (2019).

[7] S. Ran, I.-L. Liu, Y. S. Eo, D. J. Campbell, P. M. Neves, W. T. Fuhrman, S. R. Saha, C. Eckberg, H. Kim, D. Graf, F. Balakirev, J. Singleton, J. Paglione, and N. P. Butch, Nat. Phys. (2019).

[8] G. Knebel, W. Knafo, A. Pourret, Q. Niu, M. Vališka, D. Braithwaite, G. Lapertot, M. Nardone, A. Zitouni, S. Mishra, I. Sheikin, G. Seyfarth, J.-P. Brison, D. Aoki, and J. Flouquet, J. Phys. Soc. Jpn. 88, 063707 (2019).

[9] W. Knafo, M. Vališka, D. Braithwaite, G. Lapertot, G. Knebel, A. Pourret, J.-P. Brison, J. Flouquet, and D. Aoki, J. Phys. Soc. Jpn. 88, 063705 (2019).

[10] A. Miyake, Y. Shimizu, Y. J. Sato, D. Li, A. Nakamura, Y. Homma, F. Honda, J. Flouquet, M. Tokunaga, and D. Aoki, J. Phys. Soc. Jpn. 88, 063706 (2019).

[11] M. Sato, Phys. Rev. B 79, 214526 (2009).

[12] M. Sato, Phys. Rev. B 81, 220504(R) (2010).

[13] L. Fu and E. Berg, Phys. Rev. Lett. 105, 097001 (2010).

[14] X.-L. Qi and S.-C. Zhang, Rev. Mod. Phys. 83, 1057 (2011).

[15] M. Sato and S. Fujimoto, J. Phys. Soc. Jpn. 85, 072001 (2016).

[16] M. Sato and Y. Ando, Rep. Prog. Phys. 80, 076501 (2017).

[17] M. Sigrist and K. Ueda, Rev. Mod. Phys. 63, 239 (1991).

[18] S. Kobayashi, K. Shiozaki, Y. Tanaka, and M. Sato, Phys. Rev. B 90, 024516 (2014).

[19] S. Kobayashi, Y. Yanase, and M. Sato, Phys. Rev. B 94, 134512 (2016).

[20] S. Kobayashi, S. Sumita, Y. Yanase, and M. Sato, Phys. Rev. B 97, 180504(R) (2018).

[21] S. Sumita, T. Nomoto, K. Shiozaki, and Y. Yanase, Phys. Rev. B 99, 134513 (2019).

[22] S.-i. Fujimori, I. Kawasaki, Y. Takeda, H. Yamagami, A. Nakamura, Y. Homma, and D. Aoki, J. Phys. Soc. Jpn. 88, 103701 (2019).

[23] Q. Niu, G. Knebel, D. Braithwaite, D. Aoki, G. Lapertot, G. Seyfarth, J.-P. Brison, J. Flouquet, and A. Pourret, arXiv: 1907.11118.

[24] P. Blaha, K. Schwarz, G. K. H. Madsen, D. Kvasnicka, J. Luitz, R. Laskowski, F. Tran, and L. D. Marks, *WIEN2k, An Augmented Plane Wave+Local Orbitals Program for Calculating Crystal Properties* (Karlheinz Schwarz, Techn. Universität, Wien, Austria, 2018).

[25] V. I. Anisimov, J. Zaanen, and O. K. Andersen, Phys. Rev. B **44**, 943 (1991).

[26] See Supplemental Material at http://link.aps.org/supplemental/10.1103/PhysRevLett.123.217001 for details, which includes Refs. [27–36].

[27] A. J. K. Haneveld and F. Jellinek, J. Less Common Metals **21**, 45 (1970).

[28] M. T. Czyżyk and G. A. Sawatzky, Phys. Rev. B **49**, 14211 (1994).

[29] V. I. Anisimov, I. V. Solovyev, M. A. Korotin, M. T. Czyżyk, and G. A. Sawatzky, Phys. Rev. B **48**, 16929 (1993).

[30] A. I. Liechtenstein, V. I. Anisimov, and J. Zaanen, Phys. Rev. B **52**, R5467 (1995).

[31] E. P. Wigner, *Group Theory and Its Application to the Quantum Mechanics of Atomic Spectra* (Academic Press, New York, 1959).

[32] C. Herring, Phys. Rev. **52**, 361 (1937).

[33] T. Inui, Y. Tanabe, and Y. Onodera, *Group Theory and Its Applications in Physics*, Springer Series in Solid-State Sciences Vol. 78 (Springer-Verlag Berlin Heidelberg, Berlin, Heidelberg, 1990).

[34] C. J. Bradley and A. P. Cracknell, *The Mathematical Theory of Symmetry in Solids* (Oxford University Press, Oxford, 1972).

[35] K. Shiozaki, M. Sato, and K. Gomi, Atiyah-Hirzebruch spectral sequence in band topology: General formalism and topological invariants for 230 space groups, arXiv:1802.06694.

[36] A. Altland and M. R. Zirnbauer, Phys. Rev. B **55**, 1142 (1997).

[37] T. Yoshida, A. Daido, N. Kawakami, and Y. Yanase, Phys. Rev. B **99**, 235105 (2019).

[38] G. E. Volovik and L. P. Gor'kov, Pis'ma Zh. Eksp. Teor. Fiz. **39**, 550 (1984).

[39] G. E. Volovik and L. P. Gor'kov, Zh. Eksp. Teor. Fiz. **88**, 1412 (1985).

[40] P. W. Anderson, Phys. Rev. B **30**, 4000 (1984).

[41] V. G. Yarzhemsky and E. N. Murav'ev, J. Phys. Condens. Matter **4**, 3525 (1992).

[42] M. R. Norman, Phys. Rev. B **52**, 15093 (1995).

[43] T. Micklitz and M. R. Norman, Phys. Rev. B **80**, 100506(R) (2009).

[44] T. Nomoto and H. Ikeda, J. Phys. Soc. Jpn. **86**, 023703 (2017).

[45] T. Micklitz and M. R. Norman, Phys. Rev. Lett. **118**, 207001 (2017).

[46] S. Sumita, T. Nomoto, and Y. Yanase, Phys. Rev. Lett. **119**, 027001 (2017).

[47] S. Sumita and Y. Yanase, Phys. Rev. B **97**, 134512 (2018).

[48] R. Joynt and L. Taillefer, Rev. Mod. Phys. **74**, 235 (2002).

[49] G. Nakamine, S. Kitagawa, K. Ishida, Y. Tokunaga, H. Sakai, S. Kambe, A. Nakamura, Y. Shimizu, Y. Homma, D. Li, F. Honda, and D. Aoki, J. Phys. Soc. Jpn. **88**, 113703 (2019).

[50] Y. Yanase, T. Jujo, T. Nomura, H. Ikeda, T. Hotta, and K. Yamada, Phys. Rep. **387**, 1 (2003).

[51] Y. Xu, Y. Sheng, and Y. Feng Yang, following Letter, Phys. Rev. Lett. **123**, 217002 (2019).

[52] A. B. Shick and W. E. Pickett, Phys. Rev. B **100**, 134502 (2019).

[53] T. Metz, S. Bae, S. Ran, I.-L. Liu, Y. S. Eo, W. T. Fuhrman, D. F. Agterberg, S. Anlage, J. Butch, and N. P. Paglione, arXiv:1908.01069.